Fragile-strong behavior in the As_xSe_{1-x} glass forming system in relation to structural dimensionality

Guang Yang,[1,2] Ozgur Gulbiten,[3] Yann Gueguen,[2] Bruno Bureau,[1] Jean-Christophe Sangleboeuf,[2] Claire Roiland,[1] Ellyn A. King,[3] and Pierre Lucas[3,*]

[1]*UMR CNRS 6226 Sciences chimiques, Groupe Verres et Céramiques, Université de Rennes I, Campus de Beaulieu, 35042 Rennes Cedex, France*

[2]*LARMAUR ERL CNRS 6274, Université de Rennes 1, Campus de Beaulieu, 35042 Rennes Cedex, France*

[3]*Department of Materials Science and Engineering, University of Arizona, 4715 E. Fort Lowell Road, Tucson, Arizona 85712, USA*

(Received 19 January 2012; revised manuscript received 20 March 2012; published 10 April 2012)

A series of physical properties have been measured throughout and above the glass transition for the whole As_xSe_{1-x} system, including the activation for viscous flow E_η, the activation energy for enthalpy relaxation E_H, and the activation energy for structural relaxation E_a obtained by specific heat spectroscopy. All properties show a double minimum at an average coordination number $\langle r\rangle = 2.3$ and $\langle r\rangle = 2.5$ with a local maximum at $\langle r\rangle = 2.4$. This is in stark contrast to the physical properties previously measured on the same samples at room temperature and which instead show a single minimum centered at $\langle r\rangle = 2.4$. The observed trend is consistent with the dimensionality of the network derived from structural data obtained by nuclear magnetic resonance. An analysis of the complex heat capacity also reveals a bimodal relaxation process in As-rich glasses, which explains why they are kinetically fragile but appear thermodynamically strong. Finally, these results demonstrate that previous observations of an "intermediate phase" in As_xSe_{1-x} glasses near $\langle r\rangle = 2.3$ is associated with the high temperature behavior of the glassy network and should be interpreted in terms of the temperature dependence of structural constraints rather than the number of constraints in the room-temperature glass.

DOI: 10.1103/PhysRevB.85.144107 PACS number(s): 61.43.Dq, 81.05.Gc

I. INTRODUCTION

Due to the similar electronegativity of their component elements, chalcogenide glasses are widely regarded as amorphous covalent networks composed of atoms linked by a specific number of directional bonds set by Mott's 8-N rule.[1,2] This description enables one to compute the number of angular and bond constraints associated with each atom simply based on its valence.[3] Following this counting scheme Thorpe showed that networks with an average number of covalent bonds per atom equal to $\langle r\rangle = 2.4$ should have an equal number of constraints and degrees of freedom.[4,5] These glasses were therefore expected to exhibit optimal physical properties in comparison to glasses with greater or lower average coordination $\langle r\rangle$. Many covalent systems have since then been investigated, and in many cases extrema in physical properties were demonstrated near $\langle r\rangle = 2.4$.[6–10] In particular, the As_xSe_{1-x} glass forming system was recently shown to exhibit a sharp extremum at $\langle r\rangle = 2.4$ for a wide range of physical, mechanical, and spectroscopic properties including the density ρ, Young's modulus E, shear modulus G, bulk modulus K, Poisson's ratio ν, as well as the intensity and position of the $AsSe_3$ pyramidal Raman mode.[11] All these properties were measured at room temperature and indicated a single extremum at $\langle r\rangle = 2.4$. Conversely, measurements performed on the As_xSe_{1-x} system at higher temperatures throughout and above the glass transition domain appear to exhibit a minimum at a lower coordination number near $\langle r\rangle = 2.3$.[12–15] The fragility parameter m was estimated by Musgraves *et al.*[12] and showed a clear minimum at 30As%, which was interpreted in terms of entropy of mixing between Se_2 and $AsSe_{3/2}$ structural units. The activation entropy for viscous flow was measured by Nemilov[13,14] and also showed a minimum near $\langle r\rangle = 2.3$. This parameter is indicative of the curvature of the viscosity-temperature plot and can be regarded as a measure of the fragility. Finally, Georgiev *et al.* also observed a minimum near $\langle r\rangle = 2.3$ for the nonreversing component of the heat flow measured by modulated differential scanning calorimetry (MDFC) while heating throughout the glass transition.[15] This minimum was interpreted as the result of "self organization" of the glassy network, which leads to a rigid but unstressed structural domain named the "intermediate phase."

In the present paper a range of physical properties were measured throughout and above the glass transition for the whole As_xSe_{1-x} system. A double minimum is observed near $\langle r\rangle = 2.3$ and $\langle r\rangle = 2.5$ in stark contrast to the room temperature glassy behavior. The minimum at $\langle r\rangle = 2.3$ is consistent with previous high temperature measurements,[12–15] and these results demonstrate that measurements performed above the glass transition where many constraints are broken are not indicative of the corresponding solid glass properties.

II. EXPERIMENT

High purity As_xSe_{1-x} glass rods of composition $x = 0$, 0.10, 0.15, 0.20, 0.25, 0.30, 0.35, 0.40, 0.45, 0.50, 0.55, and 0.60 were prepared using a high vacuum method previously described in detail.[11] The amorphous nature of each sample was confirmed by x-ray diffraction (XRD) analysis, and the overall glass homogeneity was verified optically with a thermal-imaging camera. The composition of each sample was analyzed by energy-dispersive spectroscopy using a JEOL JSM 6301 electron microscope. The glass viscosity was measured by indentation method using homemade equipment operating up to 1200 °C. Details about this apparatus can be found in Refs. 16 and 17. The indentation tests were performed on mirror-polished samples. The viscosity (η) was measured in air using a spherical indenter (sapphire) and the following

equation:

$$\eta = \frac{3P}{16\sqrt{R}}\left(\frac{du^{\frac{3}{2}}(t)}{dt}\right)^{-1},$$

where R is the indenter radius (750 μm), P the constant load applied, and u the penetration depth of the indenter. The load was maintained long enough (up to 3 hours below T_g) to ensure that the stationary creep regime was reached. Because below T_g glasses are out of equilibrium, the samples were kept at constant temperature for at least 1 hour before starting the viscosity measurements. Thus, before measuring a viscosity of 10^{13} Pa.s, a glass is kept at least 2–3 hours at the testing temperature (1–2 hours to reach the equilibrium, 1–2 hours to reach the stationary creep regime).

The activation energy for viscous flow E_η was determined by fitting the viscosity data with the following Arrhenius equation: $\eta = A_\eta \exp[E_\eta/(RT)]$ where T is the temperature, A_η is the pre-exponential factor, and R is the gas constant. Differential scanning calorimetry (DSC) was performed with a DSC1 from Mettler Toledo. The temperature was calibrated with an indium and zinc standard. Each sample was about 10 mg and held in an aluminum pan. An empty aluminum pan was used as a reference. The activation energy for enthalpy relaxation E_H was obtained following Moynihan's method.[18,19] Each sample was heated and equilibrated far above T_g then cooled far below T_g and reheated at the same rate. The procedure was repeated for rates ranging from 3 °C/min to 30 °C/min. The activation energy was estimated from the shift in T_g with heating rate. The width of the glass transition ΔT_g was measured as the difference between the onset and end of the glass transition.[20,21] The difference in heat capacity ΔC_p between the glass and the liquid was measured as the difference between the liquid line and solid line of the DSC thermogram at the glass transition. Specific heat spectroscopy was performed using a modulated differential scanning calorimeter (MDSC) Q1000 from TA Instruments. The temperature was calibrated with an indium standard, and the enthalpy was calibrated with a sapphire standard. Each sample was about 10–15 mg and held in a hermetic aluminum pan. An empty aluminum pan was used as a reference. Samples were heated and equilibrated above the glass transition and cooled at 3 °C/min. Samples were then reheated at a rate of 3 °C/min with a modulated temperature ramp at an amplitude of 3 °C. The complex heat capacity was then determined from the modulated signal to obtain the real part C_p' and the imaginary part C_p'' of the complex heat capacity C_p^*, as shown in Fig. 1.[22–24] The activation energy for structural relaxation E_a was then obtained from the shift of the C_p'' peak measured for temperature oscillation frequencies ranging from 0.01 Hz to 0.005 Hz (or periods ranging from 100s to 200s).

^{77}Se ($I = 1/2$) magic-angle spinning (MAS) nuclear magnetic resonance (NMR) experiments were performed on a Bruker Avance 300 spectrometer (7.1 T) operating at Larmor frequency of 57.3 MHz for ^{77}Se using a 4-mm double-resonance probe head. The chemical shift was calibrated with a saturated solution of Me_2Se in $CdCl_3$. Due to the low concentration and sensitivity of ^{77}Se, several thousand scans were accumulated, and each spectrum was acquired over several days. Experimental parameters for the NMR experiment have been previously described in more detail.[11]

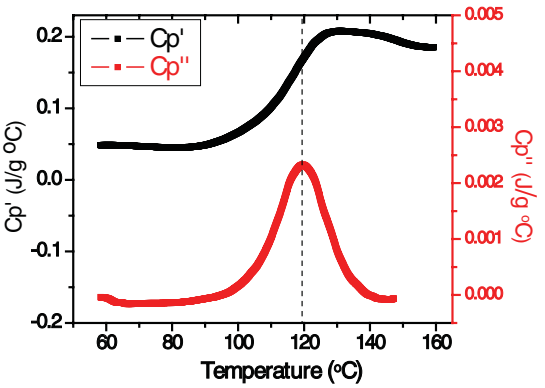

FIG. 1. (Color online) Real part C_p' and imaginary part C_p'' of the complex heat capacity C_p^* for an $As_{50}Se_{50}$ glass sample obtained from the modulated MDSC signal collected at a rate of 3 °C/min with a frequency of 0.005 Hz and amplitude of 3 °C.

III. RESULTS

A. Activation energies

1. Activation energy for viscous flow

Figure 2(a) shows the viscosity-temperature plot near the glass transition for five representative As_xSe_{1-x} samples. The viscosity is shown as a T_g-scaled Arrhenius plot in a way similar to Angell's fragility diagrams.[25,26] In the limited range of temperature near T_g, the plots show a linear dependence and can be fitted with a simple Arrhenius equation to determine the activation for viscous flow E_η. Figure 2(a) suggests a greater activation energy for the As_2Se_3 sample (40%As) in comparison to the surrounding compositions. Indeed Fig. 2(b) reports the values of E_η for all compositions and clearly indicates a local maximum in activation energy for As_2Se_3 at $\langle r\rangle = 2.4$ and two local minima near $\langle r\rangle = 2.3$ and $\langle r\rangle = 2.5$.

2. Activation energy for enthalpy relaxation

The activation energy for enthalpy relaxation E_H was estimated from the shift in T_g when measured at cooling/heating rates Q varying over one order of magnitude. Following Moynihan's method, the slop of the $\ln Q$ vs $1000/T_g$ plot is equal to E_H/R, where R is the gas constant. Figure 3(a) shows the linear dependence of $\ln Q$ vs $1000/T_g$ and the linear regression used to estimate E_H for an $As_{50}Se_{50}$ sample. The set of E_H values for all compositions is shown on Fig. 3(b). The compositional trend for E_H is very similar to that of E_η and also shows a local maximum at $\langle r\rangle = 2.4$ for As_2Se_3 and two local minima near $\langle r\rangle = 2.3$ and $\langle r\rangle = 2.5$. A correlation between E_H and E_η have been previously pointed out by Moynihan.[19]

3. Activation energy for structural relaxation by MDSC

Figure 4(a) shows the imaginary heat capacity of an $As_{50}Se_{50}$ sample recorded at increasing temperature oscillation frequency. The imaginary part of the heat capacity

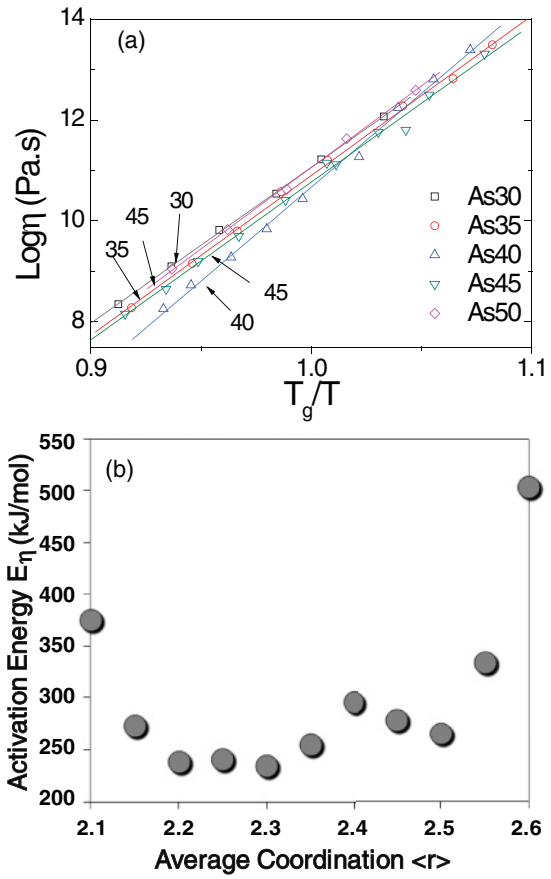

FIG. 2. (Color online) (a) T_g-scaled Arrhenius plot of the viscosity of five representative As_xSe_{1-x} samples around the As_2Se_3 composition (40%As) showing greater activation energy for this composition. (b) Activation energy for viscous flow E_η for all As_xSe_{1-x} samples.

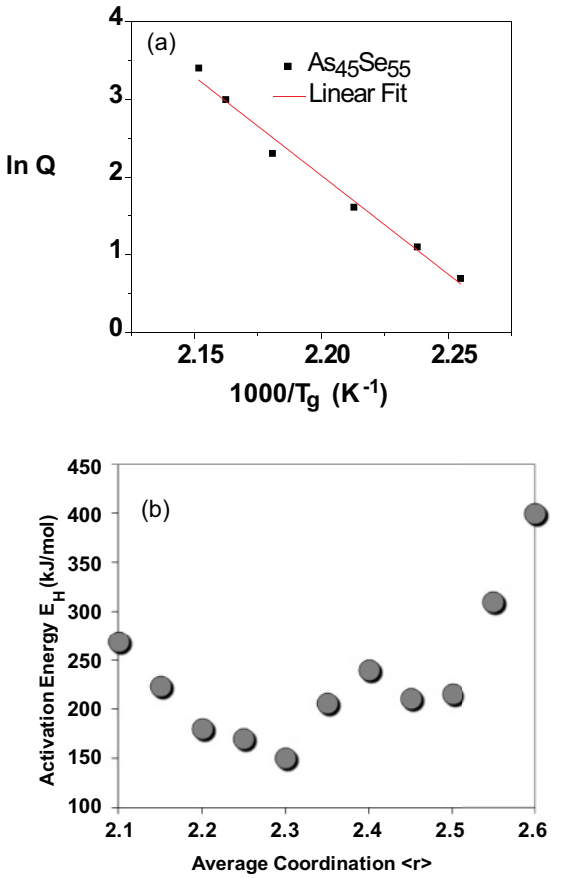

FIG. 3. (Color online) (a) Plot of the shift in T_g when measured at different cooling/heating rates Q (in K/min). The slop of the ln$Q$ vs $1000/T_g$ plot is equal to E_H/R where R is the gas constant and E_H is the activation energy for enthalpy relaxation. (b) Activation energy for enthalpy relaxation E_H for all As_xSe_{1-x} samples.

represents the time lag between the oscillating temperature change imposed by the instrument and the oscillating temperature response of the sample. The instrumental oscillation frequency is on the order of 0.01 Hz, hence at temperatures far below the glass transition temperature the time lag is zero because only atomic vibrations are involved in the heat transfer and their response is virtually instantaneous (at least in comparison to the temperature oscillation frequency). At temperatures far above the glass transition the lag is also zero because the heat transfer is now associated with molecular translations, which can also respond much faster than the temperature oscillation. On the other hand, throughout the glass transition, the heat transfer is associated with structural rearrangements having a relaxation time in the order of 100 s that result in a time lag between the input and output temperature oscillations. This time lag can therefore be used to probe the kinetic of structural processes throughout the glass transition. Figure 4(a) shows that when higher oscillation frequencies are imposed on the sample, the response is shifted to higher temperatures where the structural relaxation time is shorter. It can be shown that a linear relationship exists between the oscillation time constant defined as the inverse oscillation frequency and the temperature of maximum structural response. The linear relationship between lnω and T_ω is shown in Fig. 4(b), where ω is the temperature modulation frequency and T_ω is the temperature at the peak of the imaginary part C_p'' for an $As_{50}Se_{50}$ sample. The slope of this line then permits to determine the activation energy for structural relaxation E_a, which reflects the kinetics of structural processes in the glass near T_g.[23,24] The set of E_a values for all compositions is shown on Fig. 4(c). Again, the compositional trend for E_a is very similar to that of E_η and E_H and also show a local maximum at $\langle r\rangle = 2.4$ for As_2Se_3 and two local minima near $\langle r\rangle = 2.3$ and $\langle r\rangle = 2.5$.

B. Fragility parameters

By definition, fragile glass formers have a steep non-Arrhenius viscosity-temperature dependence near T_g as opposed to the near-Arrhenius behavior of strong systems. Upon reheating above T_g, the structures of fragile systems tend to largely collapse within small temperature increments and gain a great number of degrees of freedom that can contribute toward a high jump in heat capacity. This is the case of systems in which structural integrity relies largely on Van der Waals forces (typical of molecular liquids, the most fragile of all glassy systems). On the other hand, strong systems with covalent networks of higher dimensionality do not collapse easily and exhibit wide and shallow T_g because the

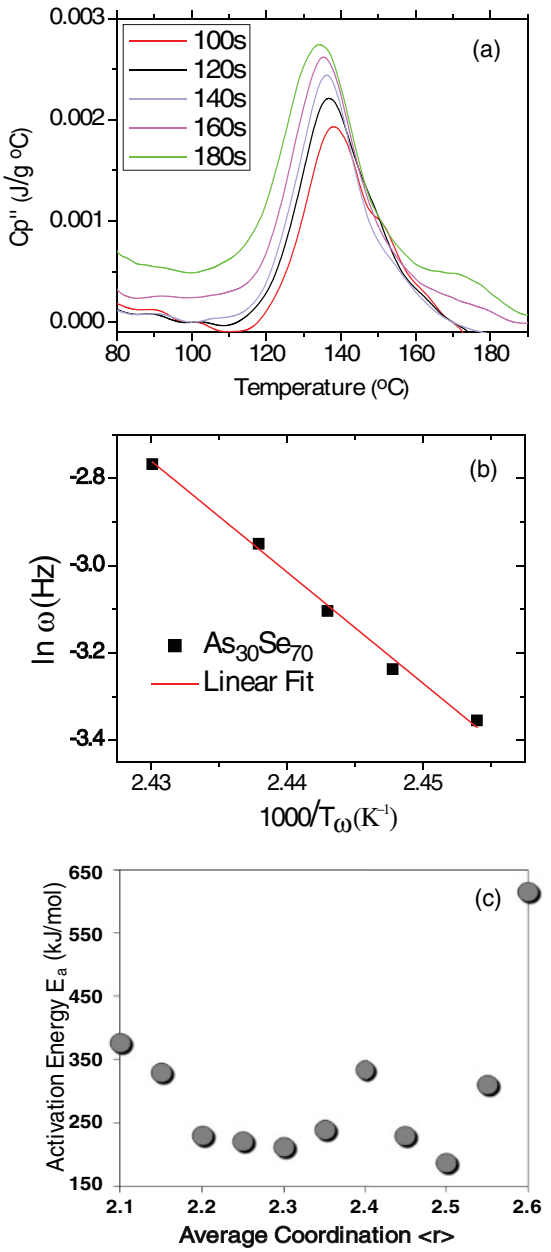

FIG. 4. (Color online) (a) Imaginary heat capacity C_p'' of an $As_{30}Se_{70}$ sample recorded at increasing temperature oscillation frequency with a heating rate of 3 °C/min and an amplitude of 3 °C. (b) Plot of the shift of the C_p'' peak with increasing temperature modulation frequency. (c) Activation energy for structural relaxation E_a obtained from MDSC for all As_xSe_{1-x} samples.

network character is retained even at high temperature (typical of covalent networks such as SiO_2 glass). Two common approaches for estimating the fragility of glass formers are then the jump in heat capacity ΔC_p and the width of the glass transition ΔT_g normalized by T_g.[21,27–29] ΔC_p and $\Delta T_g/T_g$ have an inverse dependence as expected from the standard trends in strong/fragile systems. In order to underline the composition dependence of the fragility in the As_xSe_{1-x} system, Fig. 5(a) shows ΔC_p and $\Delta T_g/T_g$ with an inverted ordinate axes. Following a similar trend to that of the activation energies, the two fragility parameters show a first minimum

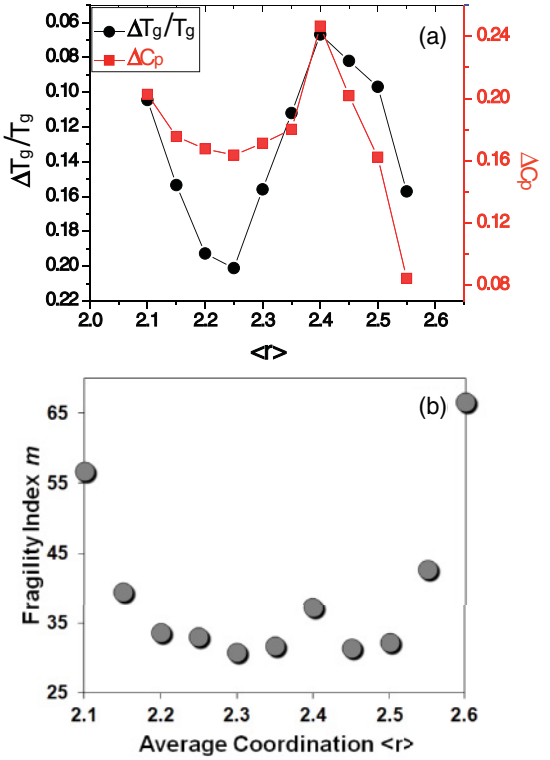

FIG. 5. (Color online) (a) Fragility indicators ΔC_p and $\Delta T_g/T_g$ obtained from DSC measurements for the As_xSe_{1-x} system. (b) Fragility index m obtained from viscosity measurements for the As_xSe_{1-x} system.

near $\langle r\rangle = 2.25$ and a maximum at $\langle r\rangle = 2.4$, however, the fragility parameters drop abruptly at higher As content. A similar trend was previously observed by Wagner *et al.* for ΔC_p.[30]

The fragility of network glass formers has long been correlated with the average coordination number $\langle r\rangle$, and it is generally observed that the fragility of chalcogenide glasses is high for under-constrained and over-constrained glasses, while it is lower for ideally constrained glasses.[9,27,28,31,32] However it must be pointed out that these previous fragility measurements were derived from viscosity data and reflect the departure from Arrhenius behavior of the viscosity-temperature plot, which is commonly quantified using the fragility index m. This kinetic fragility index can also be derived from the activation energy E_η and the T_g according to the following equation[33,34]

$$m = \frac{E_\eta}{RT_g \ln(10)},$$

where R is the gas constant. The fragility index m was obtained this way for all As_xSe_{1-x} composition using E_η values from Fig. 2(b) and T_g values from Ref. 11. The results plotted in Fig. 5(b) show a sharp increase in fragility for As-rich samples in stark contrast to the trend obtained for ΔC_p and $\Delta T_g/T_g$. These results indicate that As-rich glasses are kinetically fragile and that their viscosity rapidly collapses with increasing temperature while they also simultaneously exhibit a shallow and spread-out glass transition and appear thermodynamically strong. The origin of this apparent contradiction may be found in the structure of the glasses, as will be shown below.

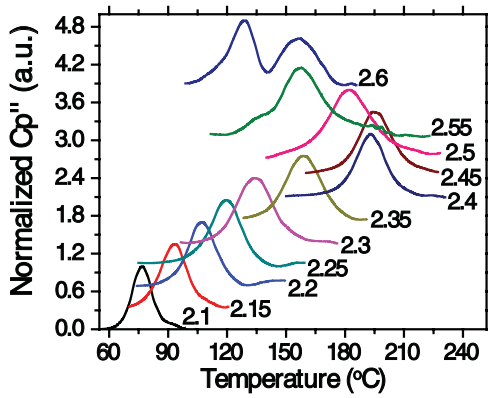

FIG. 6. (Color online) Imaginary heat capacity C_p'' of all As_xSe_{1-x} samples collected at a rate of 3 °C/min with a frequency of 0.005 Hz and amplitude of 3 °C.

C. Correlation between structure, kinetic, and fragility

Specific heat spectroscopy is an effective tool for studying the structural dynamic of network glasses. As mentioned previously the imaginary heat capacity C_p'' measures the response of the glass to an imposed temperature oscillation and therefore permits to probe the kinetics of structural rearrangements with increasing temperature. The structural relaxation time is directly related to temperature according to the Tool-Narayanaswamy-Moynihan (TNM) equation.[18,19] Hence the shape of the C_p'' peak permits to probe the relaxation profile of structural units in the glass. The C_p'' peaks for all As_xSe_{1-x} compositions are plotted in Fig. 6 and reveal two interesting features. First, all peaks show a nearly Gaussian profile except for the As-rich compositions which display a bimodal profile that becomes more pronounced with increasing As content. And second, the width of the C_p'' peak appears to follow a trend similar to that of the fragility. This characteristic is quantified in Fig. 7 using the Full Width at Half Maximum (FWHM) obtained from fitting each peak with a Gaussian, as shown in Fig. 7(a). The resulting trend depicted in Fig. 7(b) indeed indicates a correlation between the FWHM and the thermodynamic fragility estimated from ΔC_p and $\Delta T_g/T_g$. The last two compositions, $As_{55}Se_{45}$ and $As_{60}Se_{40}$, could not be fitted with a single Gaussian but in effect would be much broader.

C_p'' correlates with the structural relaxation time, and from the TNM equation it can be expected that at least two distinct contributions could affect the width of the C_p'' peak. First, a high activation energy would tend to narrow down the C_p'' peak because a small increment in temperature would notably increase the relaxation time beyond the imposed temperature frequency ω thereby rapidly reducing C_p''. Conversely, a low activation energy would tend to widen the C_p'' peak. And second, widening the C_p'' peak could also result from the presence of two distinct but overlapping relaxation processes. This appears to be clearly the case in the As-rich region of the As_xSe_{1-x} system.

The origin of both of these features can be somewhat elucidated from a structural analysis conducted by NMR. A series of representative spectra are shown in Fig. 8. The assignment of ^{77}Se environments was derived from previous investigations of these gasses by 1D and 2D MAS NMR.[11,35,36]

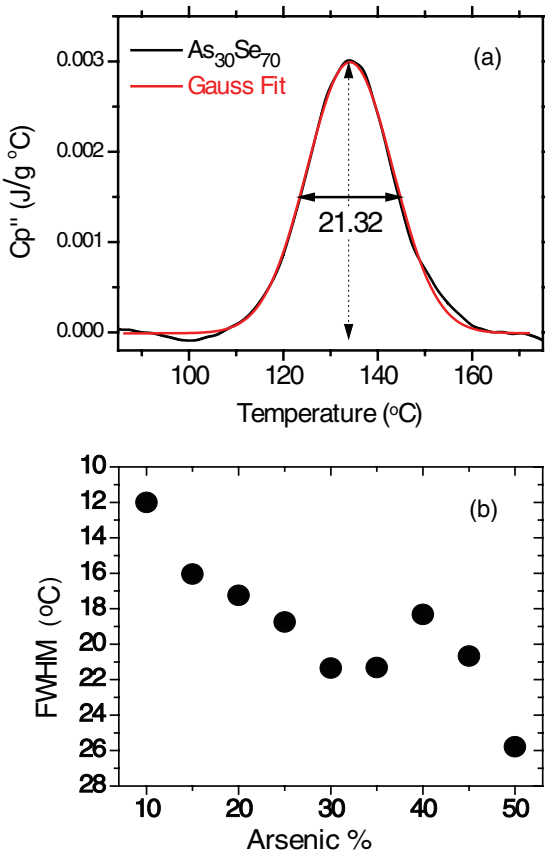

FIG. 7. (Color online) (a) Imaginary heat capacity C_p'' of an $As_{30}Se_{70}$ sample collected at a rate of 3 °C/min with a frequency of 0.005 Hz and amplitude of 3 °C and fitted with a Gaussian. The value of the FWHM is shown below the arrow. (b) FWHM of the imaginary heat capacity C_p'' of all As_xSe_{1-x} samples.

The Se-rich compositions show mainly a Se chain feature that suggest a 1D type of structure composed of lightly cross-linked chains involving significant Van der Walls interactions and leading to more fragile behavior with high activation energies. As the arsenic content increases, the structure shifts toward a 3D network where As are cross-linked by bridging Se or short Se chains, as depicted in Fig. 9 for $As_{30}Se_{70}$. This 3D character tends to lead to a strong glass behavior. When the composition reaches $As_{40}Se_{60}$ the NMR spectra indicate that the structure is entirely composed of corner sharing $AsSe_3$ pyramids that generate a sheetlike 2D structure, as depicted in Fig. 9. This structure also involves a significant amount of Van der Walls interactions between layers and leads to an increase in fragility observed in all the physical properties. Further introduction of As eventually leads to the formation of As-rich 0D cage molecules such as As_4Se_3, As_4Se_4, and As_4, as shown by NMR and which have also been unambiguously evidenced by Raman.[11] At that point the structural backbone is actually depleted in As and reverts to a mixture of a 3D network and 0D cage molecules, as illustrated in Fig. 9 for $As_{50}Se_{50}$. Finally, when the As content further increases, the backbone network reverts to a 1D/2D character mixed with an increasing amount of cage molecules. This results in the large increase in kinetic fragility observed from viscosity measurement while also producing the bimodal

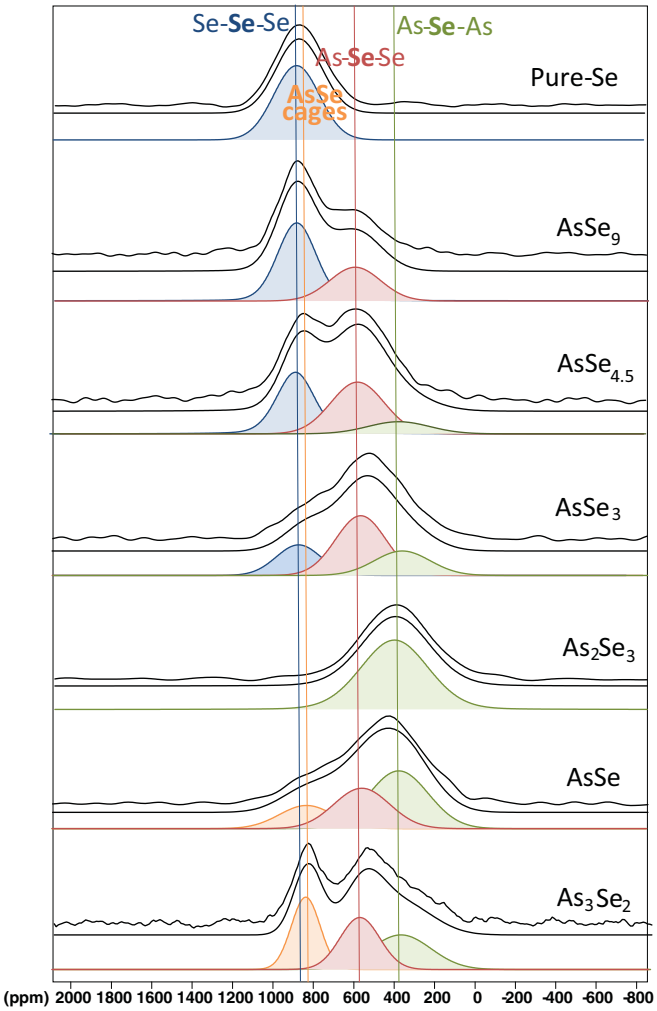

FIG. 8. (Color online) NMR spectra of selected As_xSe_{1-x} samples.

C_p'' profile observed by MDSC, which in turn generates very wide-spread glass transitions with large ΔT_g and small ΔC_p. This glass transition widening occurs because the gain in degrees of freedom is spread out over a wider temperature region as a result of the two distinct structural domains which gain mobility in two different temperature ranges. Hence these glasses appear thermodynamically strong while being kinetically fragile.

IV. DISCUSSION

The activation energies shown in Figs. 2–4 clearly indicate that the As_2Se_3 composition has a peculiar behavior within the As_xSe_{1-x} system. This composition corresponds to the ideally constrained glass of the Phillips and Thorpe theory at $\langle r \rangle = 2.4$, but it also corresponds to the stoichiometric composition where each selenium is surrounded by two arsenic atoms. Due to the triangular pyramid geometry of the trivalent arsenic, this glass has a 2D sheetlike structure composed of highly coordinated layers connected to each other through Van der Waals interactions. These highly reticulated covalent layers give rise to the elevated T_g measured in these samples,[11] but once the glass transition domain is reached the structure suddenly collapses and rapidly gains translational degrees of freedom. The corresponding structural mobility is evidenced by a large jump in heat capacity ΔC_p, as illustrated in Fig. 10, which shows normalized DSC curves for a set of compositions on both sides of As_2Se_3.

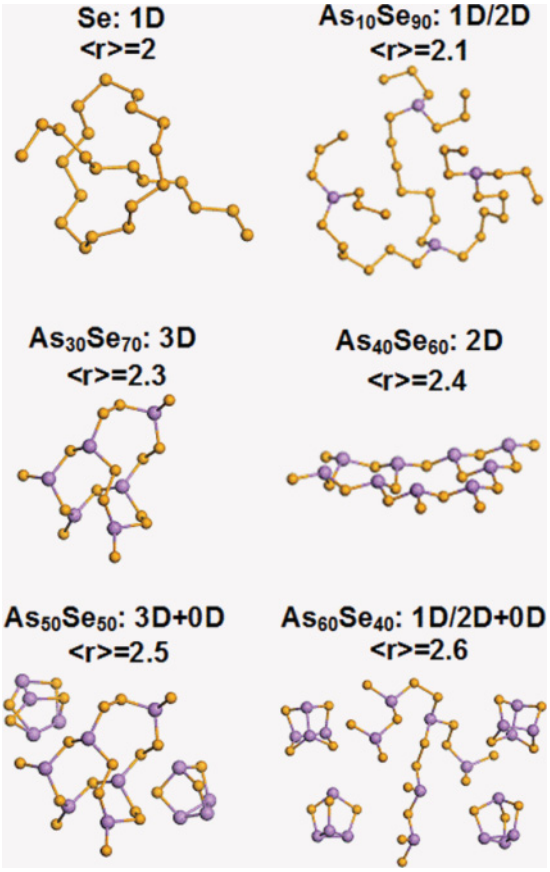

FIG. 9. (Color online) Depiction of the structure of As_xSe_{1-x} samples emphasizing the network dimentionality leading to the observed trend in physical properties.

Another notable feature of the activation energies reported in Figs. 2–4 is their symmetric trend with respect to As_2Se_3, with two local minima followed by a large increase on both sides. This symmetry reflects the dimensionality of the backbone network, which first increases to 3D then decreases towards 1D on both sides of As_2Se_3. This should be expected

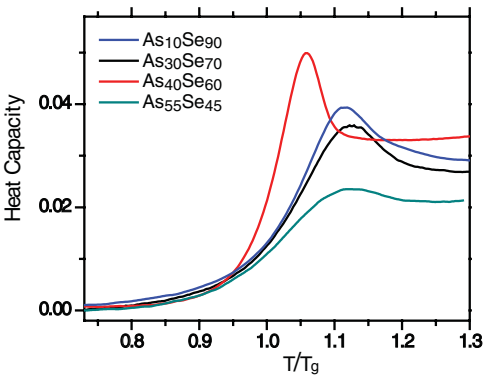

FIG. 10. (Color online) DSC curves of As_xSe_{1-x} samples on both sides of the stoichiometric composition $As_{40}Se_{60}$.

on the Se-rich compositional side where Se chains become longer but not on the As-rich side where higher coordination should increase the network reticulation. However, it is shown that the backbone network of As-rich glasses is depleted with As thereby reducing its dimensionality and increasing its fragility. This depletion in As is the result of the formation of As-rich cage molecules that should also contribute to the increase in fragility since they are bonded through weak Van der Waals interactions. The distinct contributions of the backbone and cages are made clear from the bimodal feature of the C_p'' in $As_{60}Se_{40}$ (Fig. 6). Inspection of this C_p'' curve shows that the low-temperature peak is fairly narrow and can be reasonably fitted with a Gaussian while the high-temperature peak is wider and is the sum of several contributions. The low-temperature peak also shifts with oscillation frequency and was used to calculate the activation energy in Fig. 4(c) for $As_{60}Se_{40}$. In addition, the FWHM of this peak was measured at ~13, which is rather narrow in comparison to the stronger glass compositions. In fact, if this value was included in Fig. 7(b) and compared with the other samples, the trend of the FWHM would mimic very closely that of the activation energies E_a, E_η, and E_H. The low-temperature C_p'' peak is therefore assigned to the dynamic of the backbone network, which mostly controls viscous flow and structural relaxation in these glasses. The more complex high-temperature C_p'' component is then assigned to the contributions of As_4Se_3, As_4Se_4, and As_4 cages bonded through intermolecular forces. This type of weak interaction also contributes to the fragile behavior and is reminiscent of GeAsS molecular glasses reported by Sen *et al*.[37,38]

Finally, it is important to note the contrast between the low-temperature properties of As_xSe_{1-x} glasses below T_g and the corresponding high-temperature properties near T_g where structural mobility occurs. For example, the mechanical properties of the room-temperature glasses increase linearly with As% up to As_2Se_3 in a manner consistent with the mean atomic bonding energy derived from the chain-crossing model.[11] Then for higher As%, the mechanical properties decrease linearly in a manner consistent with the increasing concentration of cage molecules in the glass.[11] The overall trend in mechanical properties therefore shows a single minimum at $\langle r \rangle = 2.4$, which is notably different from the double minimum trend observed in the high-temperature properties. This difference can be understood by considering the temperature-dependence of topological constraints in these glasses. Topological models such as the rigidity percolation of Phillips and Thorpe are defined for zero temperature conditions where all constraints are frozen. However, as the temperature of the glass is raised near T_g, sufficient thermal energy is available to overcome an increasing number of constraints. It is the rate at which these constraints are broken which will then define the high-temperature properties of these glasses. Indeed, recent works by Smedskjaer and Mauro have clearly demonstrated the correlation between the temperature dependence of structural constraints and high-temperature glass properties such as the fragility.[39–42] Bauchy and Micoulaut also showed that this treatment was consistent with the results of molecular dynamic simulations at high temperature, which reveals a significant fraction of thermally broken constraints.[43] In that respect it should be pointed out that the observation of an "intermediate phase" in As_xSe_{1-x} glasses near $\langle r \rangle = 2.3$ was derived from MDSC measurements performed across the glass transition.[15] These data are then clearly correlated with the high-temperature glass properties and should therefore be interpreted in terms of the temperature dependence of structural constraints. However, this is not consistent with the observations of an "intermediate phase" that is defined for zero temperature conditions in the same way as the rigidity percolation.

V. CONCLUSIONS

High-temperature physical properties were measured for glasses from the As_xSe_{1-x} system. The activation energies E_a, E_η, and E_H show a symmetric trend with respect to As_2Se_3 with two local minima at $\langle r \rangle = 2.3$ and $\langle r \rangle = 2.5$ and a local maximum at $\langle r \rangle = 2.4$. This trend is consistent with the dimensionality of the backbone network which dictates relaxation and flow processes in these glasses. The structure first evolves from a 1D chain character to a 3D network with increasing As%. At the As_2Se_3 composition the dimensionality reverts to a 2D-layered structure which generates a local increase in fragility. For high As%, the As atoms are concentrated in cage molecules, and the resulting As depletion decreases the reticulation of the remaining glass network. At high As content the structure is composed of a lower dimension network surrounded with cage molecules which both contribute to high kinetic fragilities. However the relaxation process of these two structural domains is spread over a wide temperature range and produces very wide glass transitions giving the appearance of thermodynamically strong glasses. Overall the noticeable difference between high-temperature and low-temperature properties in these glasses underline that topological models such as the "intermediate phase" should be interpreted in terms of the temperature dependence of topological constraints.

ACKNOWLEDGMENTS

Y.G. thanks the French Ministry of Research Grant No. 25094-2007. P.L. thanks NSF-DMR under Grant No. 0806333 and NSF-ECCS under Grant No. 0901069 and the CNRS International Associated Laboratory for Materials & Optics.

*pierre@u.arizona.edu

[1] N. F. Mott and E. A. Davis, *Electronic Processes in Non-Crystalline Materials* (Clarendon Press, Oxford, 1979).
[2] S. R. Elliott, *Physics of Amorphous Materials* (Longman, New York, 1983).
[3] J. C. Phillips, J. Non-Cryst. Solids **34**, 153 (1979).
[4] M. F. Thorpe, J. Non-Cryst. Solids **57**, 355 (1983).
[5] H. He and M. F. Thorpe, Phys. Rev. Lett. **54**, 2107 (1985).
[6] G. G. Naumis, Phys. Rev. B **61**, R9205 (2000).

[7]U. Senapati and A. K. Varshneya, J. Non-Cryst. Solids **185**, 289 (1995).
[8]L. Calvez, Z. Yang, and P. Lucas, Phys. Rev. Lett. **101**, 177402 (2008).
[9]U. Senapati and A. K. Varshneya, J. Non-Cryst. Solids **197**, 210 (1996).
[10]P. Lucas, E. A. King, O. Gulbiten, J. L. Yarger, E. Soignard, and B. Bureau, Phys. Rev. B **80**, 214114 (2009).
[11]G. Yang, B. Bureau, T. Rouxel, Y. Gueguen, O. Gulbiten, C. Roiland, E. Soignard, J. L. Yarger, J. Troles, J.-C. Sangleboeuf, and P. Lucas, Phys. Rev. B **82**, 195206 (2010).
[12]J. D. Musgraves, P. Wachtel, S. Novak, J. Wilkinson, and K. Richardson, J. Appl. Phys. **110**, 063503 (2011).
[13]S. V. Nemilov, Zh. Prikl. Khim. **37**, 1020 (1964).
[14]S. Nemilov, Zh. Prikl. Khim. **36**, 1909 (1963).
[15]D. G. Georgiev, P. Boolchand, and M. Micoulaut, Phys. Rev. B **62**, R9228 (2000).
[16]C. Bernard, V. Keryvin, J.-C. Sangleboeuf, and T. Rouxel, Mech. Mater. **42**, 196 (2010).
[17]Y. Gueguen, T. Rouxel, P. Gadaud, C. Bernard, V. Keryvin, and J. C. Sangleboeuf, Phys. Rev. B **84**, 064201 (2011).
[18]C. T. Moynihan, A. J. Easteal, M. A. DeBolt, and J. Tucker, J. Am. Ceram. Soc. **59**, 12 (1976).
[19]C. T. Moynihan, S. K. Lee, M. Tatsumisago, and T. Minami, Thermochim. Acta **280–281**, 153 (1996).
[20]C. T. Moynihan, J. Am. Ceram. Soc. **76**, 1081 (1993).
[21]K. Ito, C. T. Moynihan, and C. A. Angell, Nature **398**, 492 (1999).
[22]O. Bustin and M. Descamps, J. Chem. Phys. **110**, 10982 (1999).
[23]L. Carpentier, S. Desprez, and M. Descamps, Phase Transitions **76**, 787 (2003).
[24]C. Alvarez and J. J. Moura-Ramos, Phys. Chem. Chem. Phys. **2**, 4743 (2000).
[25]C. A. Angell, J. Non-Cryst. Solids **131–133**, 13 (1991).
[26]L. M. Martinez and C. A. Angell, Nature **410**, 663 (2001).
[27]M. Tatsumisago, B. L. Halfpap, J. L. Green, S. M. Lindsay, and C. A. Angell, Phys. Rev. Lett. **64**, 1549 (1990).
[28]C. A. Angell, J. L. Green, K. Ito, P. Lucas, and B. E. Richard, J. Therm. Anal. Cal. **57**, 717 (1999).
[29]C. A. Angell, Science **267**, 1924 (1995).
[30]T. Wagner and S. O. Kasap, Philos. Mag. B **74**, 667 (1996).
[31]P. Lucas, A. Doraiswamy, and E. A. King, J. Non-Cryst. Solids **332**, 35 (2003).
[32]P. Lucas, J. Phys.: Condens. Matter **18**, 5629 (2006).
[33]R. Bohmer and C. A. Angell, Phys. Rev. B **45**, 10091 (1992).
[34]R. Bohmer, K. L. Ngai, C. A. Angell, and D. J. Plazek, J. Chem. Phys. **99**, 4201 (1993).
[35]M. Deschamps, C. Roiland, B. Bureau, G. Yang, L. LePolles, and D. Massiot, Solid State Magn. Reson. **40**, 72 (2011).
[36]B. Bureau, J. Troles, M. LeFloch, F. Smektala, G. Silly, and J. Lucas, Solid State Sci. **5**, 219 (2003).
[37]S. Sen, S. Gaudio, B. G. Aitken, and C. E. Lesher, Phys. Rev. Lett. **97**, 025504 (2006).
[38]E. L. Gjersing, S. Sen, P. Yu, and B. G. Aitken, Phys. Rev. B **76**, 214202 (2007).
[39]M. M. Smedskjaer, J. C. Mauro, R. E. Youngman, C. L. Hogue, M. Potuzak, and Y. Yue, J. Phys. Chem. B **115**, 12930 (2011).
[40]M. M. Smedskjaer, J. C. Mauro, and Y. Yue, Phys. Rev. Lett. **105**, 115503 (2010).
[41]P. K. Gupta and J. C. Mauro, J. Chem. Phys. **130**, 094503 (2009).
[42]J. C. Mauro, P. K. Gupta, and R. J. Loucks, J. Chem. Phys. **130**, 234503 (2009).
[43]M. Bauchy and M. Micoulaut, J. Non-Cryst. Sol. **357**, 2530 (2011).